Model Predictive Control with Integral Action for the Rotational Transform Profile Tracking in NSTX-U

Zeki O. Ilhan, William P. Wehner, Eugenio Schuster

***Abstract*— Active control of the toroidal current density profile is among those plasma control milestones that the National Spherical Tokamak eXperiment - Upgrade (NSTX-U) program must achieve to realize its next-step operational goals, which are characterized by high-performance, long-pulse, MHD-stable plasma operation with neutral beam heating. In this work, a previously developed physics-based control-oriented model is embedded in a feedback control scheme based on a model predictive control (MPC) strategy to track a desired current density profile evolution specified indirectly by a desired rotational transform profile. An integrator is embedded into the standard MPC formulation to account for various modeling uncertainties and external disturbances. The neutral beam powers, electron density, and total plasma current are used as actuators. The effectiveness of the proposed MPC strategy in regulating the current density profile in NSTX-U is demonstrated in closed-loop nonlinear simulations.**

I. Introduction

Current nuclear power plants operate based on nuclear fission, which produces energy through the splitting of heavy atoms like uranium. Despite its capability for large amount of energy production, nuclear fission poses serious risks due to the release of highly radioactive nuclear waste, possibility of nuclear accidents, and utilization of the technology for the development of nuclear weapons. Unlike fission, nuclear fusion is the process by which two light nuclei (usually hydrogen isotopes deuterium and tritium) collide with each other and fuse together to form a heavier nucleus (helium) and free a neutron with a vast amount of energy release as a by-product [1]. The energy released per gram of fuel in a typical fusion reaction is significantly larger than that of a typical fission reaction. Contrary to fission, fusion poses almost no risk of a catastrophic nuclear accident, produces mostly short-term, low-level, radioactive waste, and generates no material for nuclear weapons [1].

Despite all its benefits, achieving controlled fusion on Earth is challenging since it requires high temperature (10^7–$10^9 K$) and pressure in order to overcome the Coulomb repulsion force that prevents the positively charged nuclei from fusing together. Under the applied high temperature and pressure, the reactants (hydrogen isotopes) separate from their electrons and form an ionized gas called plasma, which is considered as the fourth state of matter.

The main difficulty in maintaining fusion reactions is the development of a device that can confine the hot plasma for sufficiently long time while preventing it from hitting the walls of the confining device. Among several techniques, magnetic confinement [3] is the most promising approach and it is used in tokamak machines [4]. The word "tokamak" is the Russian acronym for "toroidal chamber with magnetic coils". Therefore, in a tokamak, confinement is achieved by balancing the expansion pressure in the plasma with the forces exerted by a magnetic field generated by both the large magnetic coils around the toroidal chamber and the current flowing toroidally in the plasma [5]. In a typical tokamak device, the contours of constant pressure form nested toroidal surfaces. The magnetic field lines also lie on the constant pressure contours, and, consequently, these contours are usually referred to as magnetic flux surfaces, which marks points of constant poloidal magnetic flux, Ψ as shown in Fig.1.

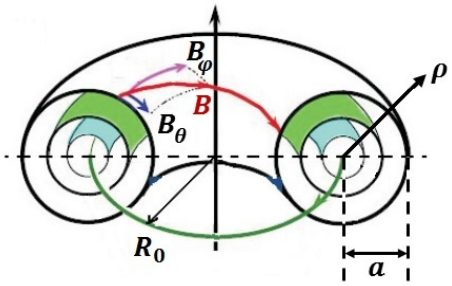

Fig. 1. Magnetic flux surfaces in a tokamak [2]. The helical magnetic field ($\vec{B}$) in a tokamak plasma is composed of toroidal ($\vec{B}_\phi$) and poloidal ($\vec{B}_\theta$) fields. The poloidal magnetic flux is defined as $\Psi = \int \vec{B}_\theta \cdot d\vec{A}_Z$, where $\vec{A}_Z$ denotes a disk of radius R that is perpendicular to a unit vector in the vertical direction. Also shown are the geometric major radius, R_0, and the minor radius, a, of the plasma.

A spherical tokamak, or a spherical torus (ST), is a special tokamak configuration with an ultra tight aspect ratio, $A = R_0/a$ [6] (see Fig. 1). Compared to a standard tokamak, the ST device extrapolates to a more compact, potentially lower-cost reactor, and the tight aspect ratio leads to a higher β value (β represents a measure of efficiency of confinement since it defines how much plasma kinetic pressure can be maintained by a given magnetic confining pressure). The National Spherical Tokamak eXperiment - Upgrade (NSTX-U), located in Princeton Plasma Physics Laboratory (PPPL) in the USA, is one of the major ST experimental facilities in the world. NSTX-U is a substantial upgrade to the former NSTX device, with significantly higher toroidal field and solenoid capabilities, and three additional neutral beam sources with significantly larger current-drive efficiency [7]. Schematics of the NSTX and NSTX-Upgrade (NSTX-U) facilities are shown in Fig. 2.

This work was supported by the U.S. Department of Energy under contract number DE-AC02-09CH11466. Z. O. Ilhan, W. P. Wehner and E. Schuster are with the Department of Mechanical Engineering and Mechanics, Lehigh University, Bethlehem, PA 18015, USA (e-mail: zoi210@lehigh.edu, schuster@lehigh.edu).

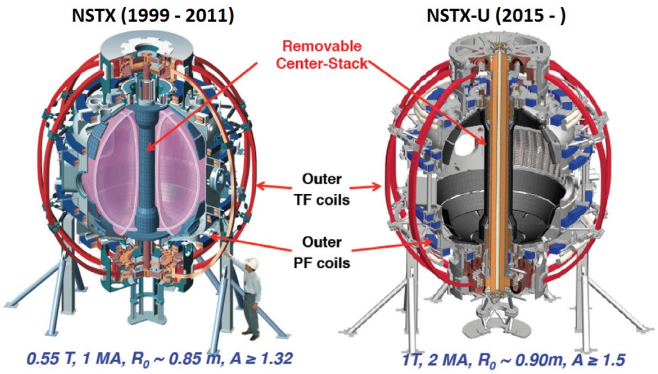

Fig. 2. Schematics of NSTX and NSTX-U devices [8]: NSTX-U retains the basic configuration of NSTX, as much of the NSTX facility is utilized including the vacuum vessel (VV) and outer toroidal field (TF) and poloidal field (PF) coils.The new centre-stack with a four times larger TF coil cross section and three times larger ohmic flux, permits the doubling of the TF from ∼0.5 to 1 T and the plasma current from 1 to 2 MA, while expanding the plasma pulse length from ∼1 to 5 s.

The rotational transform, ι is a key property affecting stability, performance, and steady-state operation in fusion plasmas. It can be shown that the value of ι on a flux surface is proportional to the plasma current enclosed by that flux surface. Therefore, control of the ι-profile is equivalent to control of the current density profile. In this work, the application of a Model Predictive Control (MPC) strategy is explored for the first time to regulate the rotational transform profile, hence the current density profile around a target profile in NSTX-U. To facilitate the control design, a nonlinear, control-oriented, physics-based model describing the temporal evolution of the rotational transform profile in NSTX-U is first put into a constrained MPC formulation. An integrator is embedded into the MPC formulation to provide offset free tracking against modeling and external disturbances. The neutral beam injectors, electron density, and the total plasma current are used as control actuators to manipulate the profile shape. The effectiveness of the proposed controller in shaping the ι-profile is shown in closed-loop nonlinear simulations.

II. First-Principles-Driven (FPD) Modeling of the Rotational Transform Profile

Any arbitrary quantity that is constant on each magnetic flux surface within the tokamak plasma can be used to index the flux surfaces, which are graphically depicted in Fig. 1. In this work, we choose the mean effective minor radius, ρ, of the flux surface, i.e., $\pi B_{\phi,0}\rho^2 = \Phi$, as the indexing variable, where Φ is the toroidal magnetic flux and $B_{\phi,0}$ is the vacuum toroidal magnetic field at the geometric major radius R_0 of the tokamak. The normalized effective minor radius is defined as $\hat{\rho} = \rho/\rho_b$, where ρ_b is the mean effective minor radius of the last closed flux surface.

Based on a magnetic description [4], the rotational transform (ι-profile) and the toroidal current density profile (j_ϕ) can be related through

$$\iota(\hat{\rho},t) = \frac{R_0\mu_0}{\hat{\rho}^2 B_\phi}\int_0^{\hat{\rho}} j_\phi(\hat{\rho}',t)\hat{\rho}'d\hat{\rho}', \tag{1}$$

where μ_0 is the permeability of the free space. Therefore, the toroidal current density can be specified indirectly by the rotational transform ι, which is also related to poloidal magnetic flux Ψ and is defined as $\iota(\hat{\rho},t) = -d\Psi/d\Phi$. Using $\Phi = \pi B_{\phi,0}\rho^2$ and $\hat{\rho} = \rho/\rho_b$, the ι-profile can also be expressed as

$$\iota(\hat{\rho},t) = -\frac{d\Psi}{d\Phi} = -\frac{2\pi d\psi}{d\Phi} = -\frac{2\pi\frac{\partial\psi}{\partial\hat{\rho}}}{\frac{\partial\Phi}{\partial\rho}\frac{\partial\rho}{\partial\hat{\rho}}} = -\frac{\partial\psi/\partial\hat{\rho}}{B_{\phi,0}\rho_b^2\hat{\rho}}, \tag{2}$$

where $\psi(\hat{\rho},t)$ is the poloidal stream function, which is closely related to the poloidal flux Ψ ($\Psi = 2\pi\psi$).

Combining (1) and (2), it can be shown that the control of the current density profile $j_\phi(\hat{\rho},t)$ is equivalent to the control of the ι-profile, which in turn is equivalent to the control of the poloidal flux gradient profile $\partial\psi/\partial\hat{\rho}$. The evolution of the poloidal magnetic flux is given in normalized cylindrical coordinates by the magnetic diffusion equation (MDE) [9]:

$$\frac{\partial\psi}{\partial t} = \frac{\eta(T_e)}{\mu_0\rho_b^2\hat{F}^2}\frac{1}{\hat{\rho}}\frac{\partial}{\partial\hat{\rho}}\left(\hat{\rho}D_\psi\frac{\partial\psi}{\partial\hat{\rho}}\right) + R_0\hat{H}\eta(T_e)\frac{\langle\bar{j}_{ni}\cdot\bar{B}\rangle}{B_{\phi,0}}, \tag{3}$$

with boundary conditions $\left.\frac{\partial\psi}{\partial\hat{\rho}}\right|_{\hat{\rho}=1} = -\frac{\mu_0}{2\pi}\frac{R_0}{\hat{G}(1)\hat{H}(1)}I(t)$ and $\left.\frac{\partial\psi}{\partial\hat{\rho}}\right|_{\hat{\rho}=0} = 0$, where η is the plasma resistivity, T_e is the electron temperature, μ_0 is the vacuum permeability, $\bar{j}_{ni}$ is any source of noninductive current density, $\bar{B}$ is the magnetic field, $\langle\rangle$ denotes a flux-surface average, $D_\psi(\hat{\rho}) = \hat{F}(\hat{\rho})\hat{G}(\hat{\rho})\hat{H}(\hat{\rho})$, where $\hat{F}$, $\hat{G}$, $\hat{H}$ are geometric factors pertaining to the magnetic configuration of a particular plasma equilibrium, and $I(t)$ is the total plasma current.

Simplified, scenario-oriented models [10] are developed for various plasma parameters to close the MDE (3) and convert it into a control-oriented form. The simplified models of n_e, T_e, and $\eta(T_e)$ profiles take the form [11]

$$n_e(\hat{\rho},t) = n_e^{prof}(\hat{\rho})u_n(t), \tag{4}$$

$$T_e(\hat{\rho},t) = k_{T_e}(\hat{\rho})\frac{T_e^{prof}(\hat{\rho})}{n_e(\hat{\rho},t)}I(t)\sqrt{P_{tot}(t)}, \tag{5}$$

$$\eta(\hat{\rho},t) = k_{sp}(\hat{\rho})Z_{eff}/[T_e(\hat{\rho},t)^{3/2}], \tag{6}$$

where $n_e^{prof}(\hat{\rho})$ and $T_e^{prof}(\hat{\rho})$ are model reference profiles, $u_n(t)$ regulates the time evolution of the electron density, $P_{tot}(t)$ is the total power injected into the plasma, Z_{eff} is the effective atomic number of the ions in the plasma, k_{T_e} and k_{sp} are the electron temperature and resistivity profile constants, respectively [11]. The simplified model of the total noninductive current-drive in NSTX-U can be written as

$$\frac{\langle\bar{j}_{ni}\cdot\bar{B}\rangle}{B_{\phi,0}} = \sum_{i=1}^{6}\frac{\langle\bar{j}_{nbi_i}\cdot\bar{B}\rangle}{B_{\phi,0}} + \frac{\langle\bar{j}_{bs}\cdot\bar{B}\rangle}{B_{\phi,0}}, \tag{7}$$

where $\bar{j}_{bs}$ is the noninductive current generated by the bootstrap effect [11], and $\bar{j}_{nbi_i}$ is the noninductive current generated by the individual neutral beam injectors

$$\frac{\langle\bar{j}_{nbi_i}\cdot\bar{B}\rangle}{B_{\phi,0}}(\hat{\rho},t) = k_i^{prof}(\hat{\rho})j_i^{dep}(\hat{\rho})\frac{\sqrt{T_e(\hat{\rho},t)}}{n_e(\hat{\rho},t)}P_i(t), \tag{8}$$

where $i = 1, 2, ..., 6$, $P_i(t)$ represents the neutral beam injection power for each beamline, $k_i^{prof}(\hat{\rho})$ is a normalizing profile, and $j_i^{dep}(\hat{\rho})$ is a reference profile for each current-drive source [11].

By substituting the simplified scenario-oriented models for the electron density (4), electron temperature (5), plasma resistivity (6), and noninductive current drives (7)-(8) into the MDE (3), space and time functions can be separated. As a result, the MDE takes the control-oriented form

$$\frac{\partial \psi}{\partial t} = f_\eta(\hat{\rho}) u_\eta(t) \frac{1}{\hat{\rho}} \frac{\partial}{\partial \hat{\rho}} \left(\hat{\rho} D_\psi(\hat{\rho}) \frac{\partial \psi}{\partial \hat{\rho}} \right) + \sum_{i=1}^{6} f_i(\hat{\rho}) u_i(t) + f_{bs}(\hat{\rho}) u_{bs}(t) \left(\frac{\partial \psi}{\partial \hat{\rho}} \right)^{-1}, \quad (9)$$

with boundary conditions $\left.\frac{\partial \psi}{\partial \hat{\rho}}\right|_{\hat{\rho}=0} = 0$ and $\left.\frac{\partial \psi}{\partial \hat{\rho}}\right|_{\hat{\rho}=1} = -f_b u_I(t)$, where $f_b = [\mu_0 R_0]/[2\pi \hat{G}(1)\hat{H}(1)]$. The spatial functions f_η, f_i, and f_{bs} are dependent on the model profiles, whereas the time functions

$$\bar{u} = [u_\eta,\, u_1,\, u_2,\, u_3,\, u_4,\, u_5,\, u_6,\, u_{bs},\, u_I]^T \in \mathbb{R}^{9\times 1} \quad (10)$$

are the manipulated control inputs, which are nonlinear combinations of the physical actuators,

$$u = [u_n,\, P_1,\, P_2,\, P_3,\, P_4,\, P_5,\, P_6,\, I]^T \in \mathbb{R}^{8\times 1}. \quad (11)$$

The nonlinear input transformations can then be written compactly as $\bar{u} = p(u)$, where $p \in \mathbb{R}^{9\times 8}$ is a nonlinear vector function defined as

$$p_1(u) = u_\eta(t) = \left[u_n(t)\, I(t)^{-1}\, P_{tot}(t)^{-1/2} \right]^{3/2}, \quad (12)$$

$$p_{i+1}(u) = u_i(t) = \left[P_i(t) I(t)^{-1} P_{tot}(t)^{-1/2} \right] \quad i=1, .., 6, \quad (13)$$

$$p_8(u) = u_{bs}(t) = \left[u_n(t)^3\, I(t)^{-1}\, P_{tot}(t)^{-1/2} \right]^{1/2}, \quad (14)$$

$$p_9(u) = u_I(t) = I(t), \quad (15)$$

where $P_{tot}(t) = \sum_{k=1}^{6} P_k(t)$ represents the total NBI power.

The ι-profile is directly related to the poloidal flux gradient (see (2)). Therefore, if we are able to control the poloidal flux gradient profile, which we define as $\theta(\hat{\rho}, t) = \partial\psi/\partial\hat{\rho}$, we will be able to control the ι-profile, assuming the system is controllable. By differentiating (9) wrt $\hat{\rho}$, the PDE governing the evolution of $\theta(\hat{\rho}, t)$ can be written compactly as

$$\frac{\partial \theta}{\partial t} = h_0 u_\eta \theta'' + h_1 u_\eta \theta' + h_2 u_\eta \theta + f'_{bs} \frac{1}{\theta} u_{bs} - f_{bs} \frac{\theta'}{\theta^2} u_{bs} + \sum_{i=1}^{6} f'_i u_i\ , \quad (16)$$

with boundary conditions $\theta\big|_{\hat{\rho}=0} = 0$, $\theta\big|_{\hat{\rho}=1} = -f_b I(t)$, where $(.)' \triangleq \partial/\partial\hat{\rho}$ for simplicity, and

$$h_0 = D_\psi f_\eta, \quad (17)$$

$$h_1 = \left(D'_\psi + \frac{1}{\hat{\rho}} D_\psi + D'_\psi \right) f_\eta + D_\psi f'_\eta, \quad (18)$$

$$h_2 = \left(D''_\psi + \frac{1}{\hat{\rho}} D'_\psi - \frac{1}{\hat{\rho}^2} D_\psi \right) f_\eta + \left(D'_\psi + \frac{1}{\hat{\rho}} D_\psi \right) f'_\eta. \quad (19)$$

III. Model Order Reduction and Linearization

A. Model Reduction via Truncated Taylor Series Expansion

To construct a reduced-order model suitable for feedback control, the governing PDE (16) is discretized in space using the truncated Taylor series while leaving the time domain continuous. The non-dimensional spatial domain ($\hat{\rho} \in [0,\, 1]$) is divided into l radial nodes, hence, the radial grid size becomes $\Delta\hat{\rho} = 1/(l-1)$. Central finite difference formulae of $O(\Delta\hat{\rho}^2)$ are used to approximate the spatial derivatives for the interior nodes, while forward and backward finite difference approximations of $O(\Delta\hat{\rho}^2)$ are used at the left and right boundary nodes, respectively. Since equation (16) is a non-linear PDE, the discrete form of it yields a set of nonlinear ODEs, which can be represented compactly as

$$\dot{\theta}(t) = g(\theta(t), \bar{u}(t)), \quad (20)$$

where $g \in \mathbb{R}^{(l-2)\times 1}$ is a nonlinear vector function of the states, inputs, and the model parameters, $\bar{u}(t)$ represents the nonlinear inputs as defined in (10), and $\theta(t) = [\theta_1(t), \theta_2(t), ..., \theta_{l-2}(t)]^T \in \mathbb{R}^{(l-2)\times 1}$ is the discrete form of $\theta(\hat{\rho}, t)$ at the $n = l-2$ interior nodes, i.e.,

$$\theta_i(t) = \theta\left(i\Delta\hat{\rho}, t\right)\ , \qquad i = 1, 2, ..., n \quad (21)$$

B. Model Linearization

Let $\bar{u}_r(t)$ and $\theta_r(t)$ represent a set of inputs and states satisfying the nonlinear, reduced-order model (20), i.e.,

$$\dot{\theta}_r = g(\theta_r, \bar{u}_r), \quad (22)$$

where $\bar{u}_r = p(u_r)$, with u_r being the reference values of the physical actuators (11). To obtain a model suitable for control design, we define the perturbation values $\tilde{\theta}(t) = \theta(t) - \theta_r(t)$ and $\tilde{u}(t) = u(t) - u_r(t)$, where $\tilde{\theta}(t)$ is the deviation from $\theta_r(t)$, and $\tilde{u}(t)$ is the to-be-designed feedback control. A first-order Taylor series expansion of (20) can be written around θ_r and u_r as

$$\dot{\theta} = g\left(\theta_r, p(u_r)\right) + \left.\frac{\partial g}{\partial \theta}\right|_{\theta_r, u_r} (\theta - \theta_r) + \left.\frac{\partial g}{\partial p}\frac{\partial p}{\partial u}\right|_{\theta_r, u_r} (u - u_r). \quad (23)$$

By substituting $\tilde{\theta}(t)$ and $\tilde{u}(t)$ into (23) and using (22), it is possible to obtain a Linear, Time-Variant (LTV), state-space model for the perturbation dynamics as

$$\dot{\tilde{\theta}}(t) = A(t)\tilde{\theta}(t) + B(t)\tilde{u}(t)\ , \quad (24)$$

where the system jacobians are expressed compactly as

$$A(t) = \left.\frac{\partial g}{\partial \theta}\right|_{\theta_r(t), u_r(t)}, \qquad B(t) = \left.\frac{\partial g}{\partial p}\frac{\partial p}{\partial u}\right|_{\theta_r(t), u_r(t)}. \quad (25)$$

After the initial ramp-up phase of the plasma discharge, u_r and θ_r remain approximately constant, such that the system dynamics (24) can be reduced to the time-invariant system

$$\dot{\tilde{\theta}}(t) = A\tilde{\theta}(t) + B\tilde{u}(t)\ , \quad (26)$$

where $A = A(t_s)$, $B = B(t_s)$ and t_s is some time during the flat-top phase of the discharge. Note that the ι-profile and the poloidal flux gradient profile $\theta(\hat{\rho}, t) = \partial\psi/\partial\hat{\rho}$ are

related through (2). Hence, the LTI model (26) for $\tilde{\theta}$ can be converted into an LTI model for $\tilde{\iota}$ as

$$\dot{\tilde{\iota}}(t) = \overline{A}\tilde{\iota}(t) + \overline{B}\tilde{u}(t)\ , \tag{27}$$

where $\overline{A} = T^{-1}AT$, $\overline{B} = T^{-1}B$, and the transformation matrix $T \in \mathbb{R}^{n\times n}$ is defined as

$$T = -\text{diag}(B_0\rho_b^2\hat{\rho}_i)\ , \quad i = 1, 2, ..., n \tag{28}$$

where $\hat{\rho}_i = i(\Delta\hat{\rho})$.

IV. MPC Formulation with Integral Action

In addition to the state equation (27), an output equation can be defined to provide a linear combination of the states. The ι-profile dynamics is then characterized by the following LTI, discrete-time, MIMO system

$$\tilde{\iota}(k+1) = \overline{A}_d\,\tilde{\iota}(k) + \overline{B}_d\,\tilde{u}(k), \tag{29}$$

$$y(k) = \overline{C}_d\,\tilde{\iota}(k), \tag{30}$$

where $\overline{A}_d$, $\overline{B}_d$ are the discrete versions of $\overline{A}$, $\overline{B}$ in the continuous time model (27), $\tilde{u}(k) \in \mathbb{R}^{m\times 1}$ and $\tilde{\iota}(k) \in \mathbb{R}^{n\times 1}$ define the deviations from a reference input $u_r(k)$, and reference state trajectory, $\iota_r(k)$, respectively, i.e., $\tilde{u}(k) = u(k) - u_r(k)$, and $\tilde{\iota}(k) = \iota(k) - \iota_r(k)$. In equation (30), $\overline{C}_d \in \mathbb{R}^{m\times n}$ is the output matrix and $y(k) \in \mathbb{R}^{m\times 1}$ is the output vector with $m = 8$ (number of control outputs chosen equal to the number of available physical actuators). The role of the matrix $\overline{C}_d$ is to select those states, that is, those radial points of the ι-profile, where the profile control must be achieved. Hence, each row of $\overline{C}_d$ has only one nonzero element, which is equal to one and is located at the column associated with the state to be controlled.

Standard MPC algorithms do not achieve integral action [12]. However, an integral action is required in the controller to achieve offset-free tracking against modeling uncertainties and external disturbances. A method for incorporating an integrator within the MPC framework is to modify the plant so that the input is the control increment $\Delta\tilde{u}(k)$, rather than control $\tilde{u}(k)$ [13], [14], [15]. This is achieved by taking the difference of both sides of (29) to form

$$\Delta\tilde{\iota}(k+1) = \overline{A}_d\Delta\tilde{\iota}(k) + \overline{B}_d\Delta\tilde{u}(k), \tag{31}$$

where

$$\Delta\tilde{\iota}(k) = \tilde{\iota}(k) - \tilde{\iota}(k-1) \tag{32}$$

$$\Delta\tilde{u}(k) = \tilde{u}(k) - \tilde{u}(k-1) \tag{33}$$

Next, from the output equation (30) one can obtain the output increment as

$$\begin{aligned}\Delta y(k+1) &= y(k+1) - y(k)\\ &= \overline{C}_d\left(\tilde{\iota}(k+1) - \tilde{\iota}(k)\right)\\ &= \overline{C}_d\overline{A}_d\Delta\tilde{\iota}(k) + \overline{C}_d\overline{B}_d\Delta\tilde{u}(k)\end{aligned} \tag{34}$$

Finally, defining a new state vector as $x = \begin{bmatrix}\Delta\tilde{\iota}(k) & y(k)\end{bmatrix}^T$, (31) and (34) are combined to form the enlarged plant

$$x(k+1) = \widetilde{A}x(k) + \widetilde{B}\Delta\tilde{u}(k), \tag{35}$$

$$y(k) = \widetilde{C}x(k), \tag{36}$$

$$\widetilde{A} = \begin{bmatrix}\overline{A}_d & 0_{n\times m}\\ \overline{C}_d\overline{A}_d & I_{m\times m}\end{bmatrix},\ \widetilde{B} = \begin{bmatrix}\overline{B}_d\\ \overline{C}_d\overline{B}_d\end{bmatrix},\ \widetilde{C} = \begin{bmatrix}0_{n\times m}\\ I_{m\times m}\end{bmatrix}^T. \tag{37}$$

Note that the state-space equations (35)-(36) may be used to define a Prediction Model (PM) [12] of the form

$$y_{k+1|N} = O_N\widetilde{A}x(k) + F_N\Delta\tilde{u}_{k|N}\ , \tag{38}$$

where

$$y_{k+1|N} = \begin{bmatrix}y(k+1) & y(k+2) & \dots & y(k+N)\end{bmatrix}^T, \tag{39}$$

$$\Delta\tilde{u}_{k|N} = \begin{bmatrix}\Delta\tilde{u}(k) & \Delta\tilde{u}(k+1) & \dots & \Delta\tilde{u}(k+N-1)\end{bmatrix}^T, \tag{40}$$

$$O_N = \begin{bmatrix}\widetilde{C} & \widetilde{C}\widetilde{A} & \widetilde{C}\widetilde{A}^2 & \dots & \widetilde{C}\widetilde{A}^{N-1}\end{bmatrix}^T, \tag{41}$$

$$F_N = \begin{bmatrix}\widetilde{C}\widetilde{B} & 0 & 0 & 0 & \cdots & 0\\ \widetilde{C}\widetilde{A}\widetilde{B} & \widetilde{C}\widetilde{B} & 0 & 0 & \cdots & 0\\ \widetilde{C}\widetilde{A}^2\widetilde{B} & \widetilde{C}\widetilde{A}\widetilde{B} & \widetilde{C}\widetilde{B} & 0 & \cdots & 0\\ \vdots & \vdots & \vdots & \ddots & & 0\\ \vdots & \vdots & \vdots & & \ddots & 0\\ \widetilde{C}\widetilde{A}^{N-1}\widetilde{B} & \widetilde{C}\widetilde{A}^{N-2}\widetilde{B} & \dots & \dots & \widetilde{C}\widetilde{A}\widetilde{B} & \widetilde{C}\widetilde{B}\end{bmatrix}. \tag{42}$$

Note that the control objective is to track the reference profile, $\iota_r(k)$ with minimum control effort. Therefore, the performance index of the MPC formulation needs to penalize both the predicted tracking error and the predicted changes to the control input [13], taking the form [16]

$$\begin{aligned}J(k) = \sum_{i=1}^{N}\Big[&y(k+i)^TQy(k+i)\\ &+ \Delta\tilde{u}(k+i-1)^TR\Delta\tilde{u}(k+i-1)\Big],\end{aligned} \tag{43}$$

where $y \in \mathbb{R}^{m\times 1}$ is the predicted output, $\Delta\tilde{u} \in \mathbb{R}^{m\times 1}$ is the future change in the feedback control input (i.e., future feedback control increment), and N is the length of the prediction horizon. Using the PM (38), the general quadratic cost (43) can be rewritten compactly as

$$J(k) = \Delta\tilde{u}_{k|N}^TH\Delta\tilde{u}_{k|N} + 2x^T(k)f^T\Delta\tilde{u}_{k|N} + J_0, \tag{44}$$

where $H = F_N^T\widetilde{Q}F_N + \widetilde{R}$, $f = F_N^T\widetilde{Q}O_N\widetilde{A}$, and $\widetilde{Q}, \widetilde{R} \in \mathbb{R}^{Nm\times Nm}$ being diagonal matrices of Q and R, respectively. Note that the term J_0 on the RHS of (44) is a scalar depending on the initial condition, $y(k)$, not on the unknown $\Delta\tilde{u}_{k|N}$. Therefore, it is not a part of the optimization problem, and is omitted in this derivation.

A. Incorporating Constraints

Let $u_{\max} \in \mathbb{R}^{m\times 1}$ and $u_{\min} \in \mathbb{R}^{m\times 1}$ define the input limits for the actual (physical) actuators of NSTX-U. Hence, for the predicted input sequence, $u_{k|N}$, it is possible to write

$$u_{\min|N} \le u_{k|N} \le u_{\max|N}, \tag{45}$$

$$u_{\min|N} = \begin{bmatrix}u_{\min} & u_{\min} & \dots & u_{\min}\end{bmatrix}^T \in \mathbb{R}^{Nm\times 1}, \tag{46}$$

$$u_{\max|N} = \begin{bmatrix}u_{\max} & u_{\max} & \dots & u_{\max}\end{bmatrix}^T \in \mathbb{R}^{Nm\times 1}. \tag{47}$$

Note that $\tilde{u}_{k|N} = u_{k|N} - u_{r_{k|N}}$, where

$$u_{r_{k|N}} = \begin{bmatrix}u_r(k) & u_r(k+1) & \dots & u_r(k+N-1)\end{bmatrix}^T \tag{48}$$

is the reference input sequence corresponding to the future input sequence, $u_{k|N}$. Therefore, the upper and lower limits for the feedback control sequence, $\tilde{u}_{k|N}$, can be obtained by subtracting (48), from all terms of (45) as

$$\underbrace{u_{\min|N} - u_{r_{k|N}}}_{\tilde{u}_{\min_{k|N}}} \leq \tilde{u}_{k|N} \leq \underbrace{u_{\max|N} - u_{r_{k|N}}}_{\tilde{u}_{\max_{k|N}}} \tag{49}$$

Using the control increment (33) recursively, it is possible to obtain the following matrix equation

$$\tilde{u}_{k|N} = S\Delta\tilde{u}_{k|N} + c\tilde{u}(k-1) \tag{50}$$

where $S \in \mathbb{R}^{Nm\times Nm}$ is a lower triangular matrix with nonzero elements being $m \times m$ identity, I_m, and

$$c = \begin{bmatrix} I_m & I_m & \dots & I_m \end{bmatrix}^T \in \mathbb{R}^{Nm\times m} \tag{51}$$

Substituting (50) into (49), the inequality for the future feedback control increment, $\Delta\tilde{u}_{k|N}$ becomes

$$\tilde{u}_{\min_{k|N}} - c\tilde{u}(k-1) \leq S\Delta\tilde{u}_{k|N} \leq \tilde{u}_{\max_{k|N}} - c\tilde{u}(k-1) \tag{52}$$

The constraints (52) are equivalent to

$$S\Delta\tilde{u}_{k|N} \leq \tilde{u}_{\max_{k|N}} - c\tilde{u}(k-1) \tag{53}$$

$$-S\Delta\tilde{u}_{k|N} \leq -\tilde{u}_{\min_{k|N}} + c\tilde{u}(k-1) \tag{54}$$

Finally, it is convenient to rewrite (53)-(54) compactly in the linear matrix inequality $\mathcal{A}\Delta\tilde{u}_{k|N} \leq b_k$, where

$$\mathcal{A} = \begin{bmatrix} S \\ -S \end{bmatrix}, \quad b_k = \begin{bmatrix} \tilde{u}_{\max_{k|N}} - c\tilde{u}(k-1) \\ -\tilde{u}_{\min_{k|N}} + c\tilde{u}(k-1) \end{bmatrix}. \tag{55}$$

B. Quadratic Programming

To solve the integral MPC formulation, the performance index (44) with the plant model (29)-(30) should be minimized with respect to the unknown future feedback control increments, while satisfying the input constraints, i.e.,

$$\Delta\tilde{u}^*_{k|N} = \arg\min_{\Delta\tilde{u}_{k|N}} \left\{ \Delta\tilde{u}^T_{k|N} H \Delta\tilde{u}_{k|N} + 2x^T(k) f^T \Delta\tilde{u}_{k|N} \right\} \tag{56}$$

$$\text{subject to } \mathcal{A}\Delta\tilde{u}_{k|N} \leq b_k \tag{57}$$

This defines a standard Quadratic Programming (QP) problem in terms of the unknown future feedback control increments, $\Delta\tilde{u}_{k|N}$. A receding horizon strategy is used and only the first control increment $\Delta\tilde{u}^*(k)$ in the calculated $\Delta\tilde{u}^*_{k|N}$ is used for control. The optimal feedback control action to the plant (29)-(30) then becomes

$$\tilde{u}(k) = \Delta\tilde{u}^*(k) + \tilde{u}(k-1). \tag{58}$$

V. Simulation Results

Although NSTX-U has been operating since the second half of 2015, there is still not enough experimental data accumulated yet to tailor a reliable model for control design. Therefore, the model reference profiles and constants are adopted based on numerical predictions by TRANSP [17], which is a highly reliable, physics-based code for predictive tokamak analysis.

Both for modeling and control design, a reference state trajectory $\iota_r(\hat{\rho}, t)$ is generated through the open-loop TRANSP run 142301W12, which is based on NSTX-U shape and actuators, and for which the actuator requests are set to the following arbitrary constants

$$\begin{aligned} u_r(k) = u_r &= \begin{bmatrix} u_n & P_1 & P_2 & P_3 & P_4 & P_5 & P_6 & I_p \end{bmatrix}^T \\ &= \begin{bmatrix} 1.0 & 0.2 & 0.4 & 0.6 & 0.8 & 1.0 & 1.2 & 0.7 \end{bmatrix}^T \end{aligned} \tag{59}$$

Both for control design and closed-loop simulation, the non-dimensional spatial domain ($\hat{\rho} \in [0\ 1]$) is equally divided into $l = 21$ radial nodes, hence, the radial grid size is $\Delta\hat{\rho} = 0.05$. Control simulations are then carried out for $t \in [t_0\ \ t_f] = [1.0\ \ 4.0]$ s. The control sampling time is set to $T_s = 0.01$ s. Note that MPC may not guarantee closed-loop stability for arbitrary values of the prediction horizon, N. In general, the chance of getting closed-loop instability decreases with an increasing N, at the expense of an increase in computational time since the length of the unknown vector $\Delta\tilde{u}_{k|N}$ in (56)-(57) also increases with an increasing N [16]. In this case, some of the closed-loop poles of the unconstrained MPC (i.e., the eigenvalues of $\widetilde{A} + \widetilde{B}K$, where $K = -H^{-1}f$) start to cross the unit circle for $N \leq 4$. Therefore, $N = 5$ is picked to guarantee closed-loop stability without increasing the computational effort considerably.

In this closed-loop control simulation study, the initial condition perturbation rejection capability is tested during the first 1.5 seconds of the discharge by setting $\iota(t_0) = \iota_r(t_0) + 0.3\iota_r(t_0)$. In addition to an initial condition perturbation, step disturbances are also added in each input channel starting at $t = 2.5$ s., i.e.,

$$\tilde{u}(k) = \begin{cases} \Delta\tilde{u}^*(k) + \tilde{u}(k-1), & t < 2.5\,\text{s}. \\ \Delta\tilde{u}^*(k) + \tilde{u}(k-1) + u_d, & t \geq 2.5\,\text{s}. \end{cases} \tag{60}$$

where $u_d = 0.15u_r$. To seek a faster response, the cost weight matrices are set to $Q = 1000\, I_{8\times 8}$ and $R = \text{diag}(0.01, 0.005, 0.001, 0.0001, 0.01, 0.001, 0.01, 0.01)$.

At the beginning of each simulation step, k, the QP problem (56)-(57) is solved in MATLAB to obtain the future feedback control increment, $\Delta\tilde{u}_{k|N}$. Receding control strategy is used to update the feedback control according to (58). The nonlinear MDE (9) is then simulated in MATLAB with the updated control input, and the prediction horizon is shifted for the next time step.

The results of the closed-loop control simulation is provided in Fig. 3. The time evolution of the optimal physical inputs are illustrated in Figs. 3(a)-(c). The corresponding time evolution of the optimal outputs are depicted in Figs. 3(d)-(e) along with their respective targets. Note from Figs. 3(d)-(e) that in the absence of the input disturbances, the outputs are regulated around their desired values within the first 0.5 s. of the simulation. This is also reflected in Fig. 4, through the comparison of the ι-profile achieved at $t = 1.5$ s. with the desired target profile, $\iota_r(t = 1.5)$, along with the unperturbed initial profile, $\iota_r(t = 1)$, and the perturbed initial profile, $\iota(t = 1)$. Note from Fig. 3(e) that the outer states jump again at $t = 2.5$ s., which is the effect of the step disturbance inputs added at that instant. The integral MPC strategy instantly cancels the effect of these input

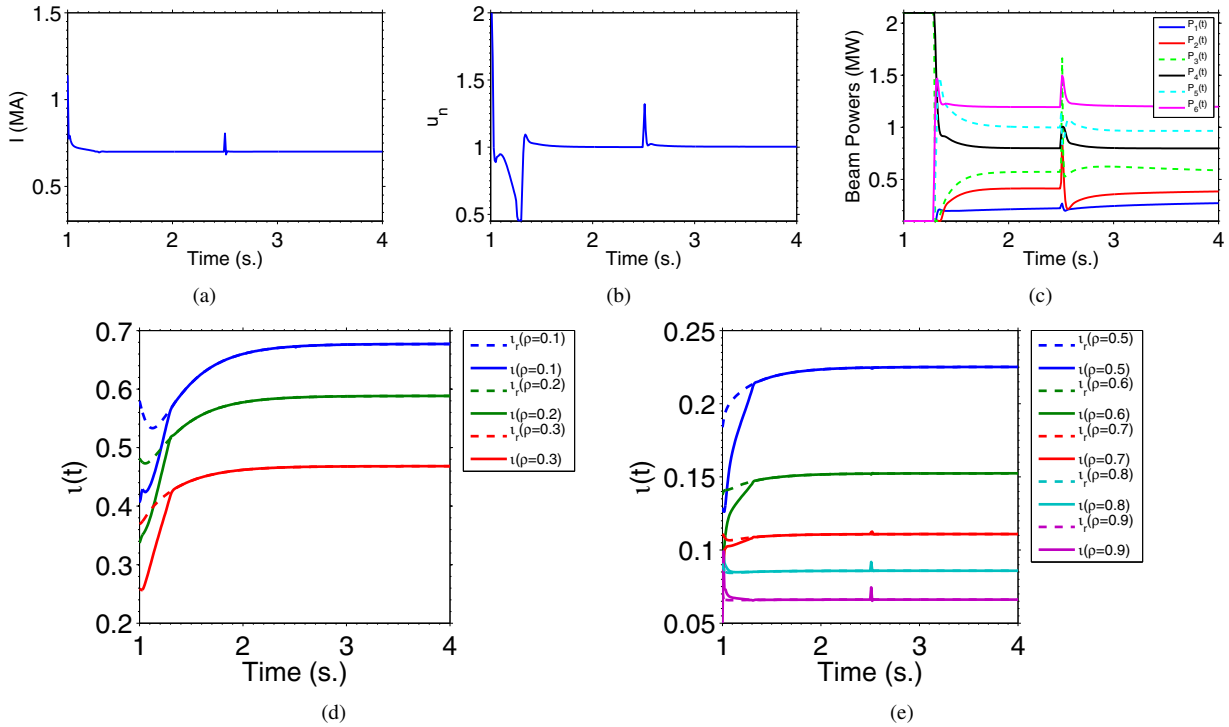

Fig. 3. Tracking simulation results: (a)-(c) Time evolution of the optimal plasma current, electron density regulation and neutral beam injection powers; (d)-(e) Time evolution of the actual outputs (solid) with their respective targets (dashed).

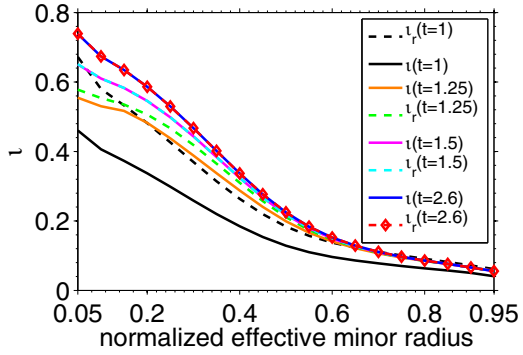

Fig. 4. Time evolution of the rotational transform (ι-profile).

disturbances, providing almost excellent profile matching at $t = 2.6$ s. in Fig. 4. Based on this simulation analysis, the proposed controller is shown to be effective in regulating the ι-profile around a target profile in NSTX-U.

VI. Conclusion and Future Work

In this work, an MPC algorithm is formulated for ι-profile tracking in NSTX-U. An integrator is added to the MPC formulation to achieve offset-free tracking against various modeling uncertainties and external disturbances. The effectiveness of the proposed controller is tested in numerical simulations based on an MDE solver. The main contribution of this work resides in the application itself since this is the first MPC application ever designed for NSTX-U for current density profile control. The next step is to experimentally test the controller once NSTX-U starts operation.

References

[1] A. Pironti and M. Walker, "Fusion, Tokamaks, and Plasma Control," *IEEE Control Systems Magazine*, vol. 25, no. 5, pp. 30–43, 2005.

[2] B. L. Tan and G. L. Huang, "Neoclassical bootstrap current in solar plasma loops," *Astronomy and Astrophysics*, vol. 453, no. 1, pp. 321–327, 2006.

[3] J. Sheffield, "The physics of magnetic fusion reactors," *Reviews of Modern Physics*, vol. 66, pp. 1015–1103, 1994.

[4] J. Wesson, *Tokamaks*. Clarendon Press, Oxford, UK, 1984.

[5] M. Ariola and A. Pironti, *Magnetic Control of Tokamak Plasmas*. Springer, 2008.

[6] J. Freidberg, *Plasma Physics and Fusion Energy*. Cambridge University Press, Cambridge, UK, 2007.

[7] S. P. Gerhardt *et al.*, "Exploration of the equilibrium operating space for NSTX-Upgrade," *Nuclear Fusion*, vol. 52, no. 8, 2012.

[8] M. Ono *et al.*, "Progress toward commissioning and plasma operation in NSTX-U," *Nuclear Fusion*, vol. 55, no. 7, 2015.

[9] Y. Ou *et al.*, "Towards model-based current profile control at DIII-D," *Fusion Engineering and Design*, vol. 82, pp. 1153–1160, 2007.

[10] J. E. Barton *et al.*, "Physics-based control-oriented modeling of the safety factor profile dynamics in high performance tokamak plasmas," *52nd IEEE CDC*, pp. 4182–4187, 2013.

[11] Z. Ilhan *et al.*, "First-principles-driven model-based optimal control of the current profile in NSTX-U," *IEEE Conference on Control Applications (CCA)*, 2015.

[12] D. D. Ruscio, "Model predictive control with integral action: a simple MPC algorithm," *Modeling, Identification and Control*, vol. 34, no. 3, pp. 119–129, 2013.

[13] M. A. Stephens *et al.*, "Model predictive control for reference tracking on an industrial machine tool servo drive," *IEEE Transactions on Industrial Informatics*, vol. 9, no. 2, pp. 808–816, 2013.

[14] D. M. Prett and C. E. Garcia, *Fundamental Process Control*. H. Brenner Ed. Butterworth, Stoneham, MA, 1988.

[15] L. Wang, *Model Predictive Control System Design and Implementation Using MATLAB*. Springer-Verlog, London, UK, 2009.

[16] J. M. Maciejowski, *Predictive Control With Constraints*. Prentice-Hall, Harlow, UK, 2002.

[17] "TRANSP Homepage," http://w3.pppl.gov/transp/, 2015.